



RESEARCH ARTICLE

Small aircraft flight trajectory optimisation using a multidisciplinary approach

M. Rostami , J. Bardin, D. Neufeld and J. Chung 

Department of Aerospace Engineering, Toronto Metropolitan University, Toronto, ON, Canada

Corresponding author: J. Chung; Email: j3chung@torontomu.ca

Received: 28 February 2024; Revised: 6 August 2024; Accepted: 17 October 2024

Keywords: aircraft performance; flight trajectory optimisation; small aircraft; multidisciplinary approach; Operative cost reduction

Abstract

In a competitive market, airlines continually seek solutions that can reduce their operational costs. Flight path optimisation is a commonly pursued approach to this but requires a large amount of data about the flight environment including the weather information, the aircraft performance and the air traffic control (ATC) requirements. Existing programmes require the user to provide this aircraft performance data in advance and are incapable of generating the information on their own. In this study, using a multidisciplinary approach and numerical optimisations, a novel standalone flight path optimiser (SAFPO) solution is proposed and developed to choose the best flight path for a flight between two points in accordance with the cost objectives. SAFPO uses its own performance calculator, predefined ATC routes, and known weather information to find the optimum flight path which minimises fuel consumption and/or flight time. The aerodynamic characteristics of the aircraft are determined using a validated semi-empirical programme called MAPLA, previously developed for light aircraft analysis. Furthermore, the optimisation process consists of a multidisciplinary-feasible (MDF) framework that employs a genetic algorithm (GA) optimiser. The resulting performance characteristics of the aircraft and the optimisation process are compared with the actual information provided within the flight manual of a Beechcraft Baron G58 aircraft. The optimisation results show that SAFPO can be used to make advances in the daily operations of small and local airlines suffering from a lack of aircraft performance data and help them to choose the scenario that best accomplishes their cost objectives.

Nomenclature

Roman symbols

C_D	drag coefficient
C_L	lift coefficient
D	drag force
dt	time step
g	gravitational acceleration
h	flight altitude
J	cost objective
$P_{\text{effective}}$	effective power imparted to the air by the propeller
P_{shaft}	power provided to the propeller via the shaft
p_{TP}	static pressure at the tropopause
p_0	sea level atmospheric pressure
R	ideal gas constant for air

ROC	rate of climb
ROD	rate of descent
S	distance travelled during the segment
SFC	specific fuel consumption of the engine
S_{ref}	wing planform area
T	thrust per each propeller
T_{req}	required thrust
T_{avail}	available thrust
T_a	predicted ambient temperature
T_{ISA}	temperature in K predicted by the international standard atmosphere
T_0	sea level atmospheric temperature
T	time required for the segment, which started counting from 0
V	true airspeed of the aircraft
V_{wind}	windspeed
W	instantaneous weight of the aircraft
W_{final}	final aircraft weight
W_{fuel}	fuel weight
W_{init}	initial aircraft weight

Greek symbols

ρ	air density
η_p	propulsive efficiency of the propeller
ΔT	ISA temperature deviation

1.0 Introduction

There are currently many small airlines operating across the globe, which face high operating costs and therefore seek to reduce them. Of these expenses, approximately 40% is the cost of fuel alone [1]. Targeting a reduction in this, a major way for airlines to minimise their operational costs comes from finding the most optimum flight route [1, 2]. A previous study by Boeing showed that, by using flight planning optimisers, a US airline with 60 single-aisle airplanes could save about 1 m US gallons of fuel per year, which equates to at least 5 m USD per year depending on the location. This, in turn, would also reduce the annual CO₂ emissions of the airline by approximately 20 m pounds [3].

To describe an aircraft flight, a flight plan is required [4]. This includes guiding a point-like object from an initial starting location to some final destination [5]. To best achieve this, flight planning optimisation tools are typically employed, which select flight routes that best accomplish the given cost objectives, typically centred around operating costs, environmental footprint and noise pollution [6–11]. Finding an optimised flight plan, however, requires a large amount of data about the flight environment including the weather information, the aircraft performance and the ATC requirements. Using this information, the flight plan optimisers are constructed to develop economic routes while ensuring that the risk of mid-air accidents remains low. In consideration of this economic goal, fuel consumption is considered for the flight, which is typically defined by fuel flow rate estimations within published aircraft manuals; most often it is also a function of ambient air temperature, flight altitude, true airspeed and gross weight [12]. Simultaneously, to comply with air traffic control, the developed routes must fly in controlled airspace and track predetermined routes identified as airways [13, 14].

As stated, the output of the optimisation process is significantly affected by weather conditions. This can change on a daily or even hourly basis. Another core discipline to be considered is aircraft performance information, which in current implementations has been required to be supplied by the operators. This comes in the form of predefined aircraft data available in the aircraft flight manual as the programmes cannot generate this performance information on their own. Accordingly, for any new aircraft, the user will need to find accurate performance information. Generally, aircraft manufacturers only provide information for general flight conditions, specifically those that would allow them to pass

the certifications requirements. Hence, the process of finding the most optimum flight route is often complicated or stunted by the lack of high-resolution information.

Drawing from this conclusion, a platform that can both generate aircraft performance data and then use it to predict optimal flight paths is quite necessary to provide the optimal flight scenario that can reduce the operating cost of small airlines. Recently, NASA released 796 programmes in different categories under the NASA Technology Transfer program. Among those, the Traffic Aware Planner (TAP) is a cockpit-based programme developed to test the concept of Traffic Aware Strategic Aircrew Requests (TASAR). TASAR provides in-flight optimised route and altitude updates that would help airlines to reduce fuel consumption and/or flight time, avoid known traffic interference, as well as weather and restricted airspace [15–19]. Furthermore, NASA is working on the flight optimisation system (FLOPS), which is a multidisciplinary programme with six primary modules of (1) weights, (2) aerodynamics, (3) propulsion data scaling and interpolation, (4) mission performance, (5) take-off and landing and (6) programme control. FLOPS can be used for conceptual and preliminary design and evaluation of aircraft concepts. It can also be used to generate aircraft performance data in different flight regimes [20, 21].

In multidisciplinary design optimisation (MDO), numerical optimisation is of interest to design a system containing a couple of disciplines [22, 23]. A couple of approaches have been proposed for MDO such as multiple-discipline-feasible (MDF), individual discipline feasible (IDF), all-at-once (AAO), concurrent subspace optimisation (CSSO), collaborative optimisation (CO), bi-level integrated system synthesis (BLISS), multidisciplinary design optimisation based on independent subspaces (MDOIS) and simultaneous analysis and design (SAND). MDF, IDF, AAO and MDOIS are considered as single-level methods using a single optimiser and directly implement the non-hierarchical structure. CSSO, BLISS and CO are multilevel methods where each level has an optimiser, and a hierarchical structure is implemented [24].

In the proposed study, the main goal is to implement MDO for flight path optimisations with the use of a validated semi-empirical method. Accordingly, the user will no longer need to use external programmes for performance calculations, as this has been included within the developed implementation.

2.0 Methodology

To develop a flight path optimiser, flight environment information is required. This includes the weather data, the aircraft performance charts and the airspace. The aircraft performance model is required to determine the best operating speed and cruise altitude at a given weight. The proposed solution fuses weather information, pre-existing flight routes and SAFPO's performance calculator to offer the best flight path to reduce fuel consumption and/or travel time. Consequently, operators are able to select the optimised cruise altitude using this information. For the purposes of comparison, here the actual performance data from the operating manual of the aircraft was also used.

2.1 Weather model and SIGMET

The weather model contains a set of weather-related information including temperature and wind speed in a four-dimensional (4D) space as longitude, latitude, altitude and time. Thunderstorms usually extend very high altitude and impact commercial flights. The convective SIGMET product is human-drawn polygons that denote regions of current convective weather that may be potentially hazardous to aircraft. They usually include information in terms of an initial position, velocity and a validity period. In this work, using the raw information from NAV Canada, a quadrilinear interpolation was performed to obtain the required data in the 4D space of longitude, latitude and altitude directions and time [25].

2.2 ATC waypoints and routes

A waypoint is a fixed geographical location expressed in longitude and latitude co-ordinates. Waypoints can be used to specify a change in direction, speed or altitude along the current path. A route or airway

is a corridor that connects two specific positions at a specific altitude. However, airlines and pilots are not completely bound to routes and waypoints when planning a flight. Here, the ATC waypoints of the proposed flight path optimiser were gathered from SkyVector [26].

2.3 Aircraft performance

In this work using MAPLA, the required characteristics for performance information were estimated. MAPLA is an enhanced semi-empirical multidisciplinary analysis programme that is developed for design optimisation and evaluation of light, general aviation, propeller-driven aircraft. MAPLA has five primary disciplines for analysis: aerodynamics; weight and balance; propulsion; performance and stability; and control. Specialised for light, propeller-driven airplanes, available state-of-the-art analytical procedures, and design data collections have been combined and modified in a unique method and automated in MAPLA. Previous investigations showed that MAPLA is able to determine the aerodynamic characteristics of light aircraft with acceptable accuracy in various configurations and flight regimes [27–33].

The operating manual of an aircraft provides tables and data for the fuel flow, operating speed and rate-of-climb (ROC) in different flight phases including cruise, climb and descent at various altitudes. Accordingly, for the cases of the actual aircraft data, a 2D-interpolation approach was used to model aircraft performance in terms of the fuel flow, airspeed and ROC as a function of the total weight and flight altitude.

In the following, the procedure used for the development of the performance module of MAPLA is presented. In the first step, an aerodynamic model function was implemented to link the lift coefficient, angle-of-attack and drag coefficient values. This function would store these values and index the relationship with a user-set flap and slat configuration that corresponded to this information. Data for this was generated by MAPLA prior to the performance analysis.

Thrust curves were also stored prior to the performance modelling in a dedicated thrust modelling function. Before the performance calculators were run, the effective thrust and power vs. true airspeed curves were stored for the maximum take-off and maximum continuous operating cases. The decision was made to store effective thrust and power, quantities which causes the aircraft to accelerate, as the power imparted to the propeller was able to simply be calculated by dividing the effective power by the propulsive efficiency:

$$P_{\text{shaft}} = \frac{P_{\text{effective}}}{\eta_p} \quad (1)$$

where P_{shaft} is the power provided to the propeller via the shaft (a known value published by engine manufacturers), $P_{\text{effective}}$ is the effective power imparted to the air by the propeller, and η_p is the propulsive efficiency of the propeller.

For this approach, a propeller aircraft with approximately constant engine shaft power was used. A constant propeller efficiency of 80% was further assumed, as was consistent with the traditional modelling approach [34]. However, more accurate results could be achieved by using manufacturer-produced charts that account for variations in advanced ratio, thrust coefficient and power coefficient. This assumption may lead to some discrepancies in the results. As thrust is required for determining the acceleration of the aircraft, this was computed using the effective propeller power:

$$T = \frac{P_{\text{effective}}}{V} \quad (2)$$

where V is the true airspeed of the aircraft.

The international standard atmosphere was used to model atmospheric conditions expected to be experienced by the aircraft during flight. For this implementation, the troposphere and tropopause were included. For altitudes below 11,000m, the following tropospheric relations were used:

$$T_{\text{ISA}} = T_0 - 0.0065h \quad (3)$$

$$p = p_0 \left(1 - 0.0065 \frac{h}{T_0} \right)^{5.2561} \quad (4)$$

where T_{ISA} is the temperature in K predicted by the international standard atmosphere, p is the ambient static pressure in Pa, h is the altitude in metres, p_0 is the sea level atmospheric pressure equal to 101,325 Pa and T_0 is the sea level atmospheric temperature equal to 288.15 K [35].

For modelling above the tropopause, the following relations were used:

$$T_{ISA} = 216.65 \quad (5)$$

$$p = p_{TP} \exp \left(-\frac{g}{RT_{ISA}} (h - 11,000) \right) \quad (6)$$

where p_{TP} is the static pressure at the tropopause equal to 22,632 Pa, g is gravitational acceleration and R is the ideal gas constant for air [35].

As the analysis was conducted using pressure altitude, no offsets were required for this quantity. To account for deviations between real atmospheric temperatures and those predicted by the ISA model, an offset was able to be given to the function. This was incorporated to the ambient temperature that the function returned with:

$$T_a = T_{ISA} + \Delta T \quad (7)$$

where T_a is the predicted ambient temperature in K, and ΔT is the ISA temperature deviation [35, 36].

The density was finally calculated using the ambient static pressure and temperature according to the ideal gas law:

$$\rho = \frac{p}{RT_a} \quad (8)$$

where ρ is the air density.

For each mission-phase, the aircraft was modelled to fly according to a speed schedule, that is a calibrated airspeed prescribed for each altitude of the flight. The calibrated airspeed target varied little across the flight envelope, and as such these values were averaged to prescribe a target speed value across a selected altitude range. As the ATC limit applied up to 10,000 ft, two altitude ranges were used to store the data: flying from 0 and 10,000 ft, and flying above 10,000 ft. During a mission segment analysis, the aircraft was assumed to always fly according to the speed schedule.

2.3.1 Climb-phase analysis

Analysis of the climb-phase of the aircraft mission was modelled using a numerical integration approach. As implemented, constant weight, speed and acceleration were assumed for 1 second time-steps, with the algorithm checking after each step whether the final altitude had been reached, the rate of climb was below the service-ceiling threshold or if the weight had gone below the operating empty weight (OWE) of the aircraft. Once the ending condition was triggered, the numerical integration was terminated and the results were given to the main trajectory optimisation algorithm.

The analysis began at a given initial altitude, with the goal climbing the aircraft up to some final altitude. For one instant in the analysis, the following steps were carried out:

1. Convert the calibrated airspeed from the speed schedule into true airspeed.
2. Find the maximum continuous effective thrust and power from the thrust model.
3. Calculate the lift coefficient.
4. Request the corresponding drag coefficient from the aerodynamic model.
5. Compute the drag force.
6. Compute the rate of climb.

Regarding the lift coefficient step, this was carried out by assuming that the lift force was approximately equal to the weight. With this assumption, the lift coefficient was computed as follows:

$$C_L = \frac{2W}{\rho V^2 S_{\text{ref}}} \quad (9)$$

where C_L is the lift coefficient, W is the instantaneous weight of the aircraft in N , ρ was the air density according to the atmospheric model, V is the true airspeed in m/s , and

S_{ref} is the wing planform area in m^2 . This value was used as an input to the aerodynamic model, which stores the drag polar, and allows for the drag coefficient to be obtained. The drag force was then computed with the following equation:

$$D = \frac{1}{2} \rho V^2 S_{\text{ref}} C_D \quad (10)$$

where D is the drag force in N , and C_D is the drag coefficient. The rate of climb for the airplane was then able to be computed with the following relationship:

$$\text{ROC} = \frac{(T - D) V}{W} \quad (11)$$

where ROC is the rate of climb in m/s , and T is the effective thrust generated by the engines and propellers. Following the calculation of the rate of climb, the value was compared against the service ceiling threshold. If the speed was lower than the threshold, the values corresponding to the previous iteration were returned as this was an invalid data point.

Passing the service ceiling check, time-stepping forward was carried out next by assuming that the thrust, speed and rate of climb were constant over the course of one second. First, the altitude of the next step was computed with:

$$h_{i+1} = h_i + \text{ROC} \cdot dt \quad (12)$$

where dt is the time-step, chosen to be one second, h_i is the altitude of the current iteration, and h_{i+1} is the altitude for the upcoming iteration [37].

The weight of the next iteration was computed by subtracting the weight consumed by the engine over the course of one second from the iteration's aircraft weight:

$$W_{i+1} = W_i - \frac{P}{\eta_p} \text{SFC} \cdot dt \quad (13)$$

where W_{i+1} is the weight of the succeeding iteration, W_i is the weight of the current iteration, SFC is the specific fuel consumption of the engine, and P/η_p is the shaft power of the engine, equal to the effective power divided by the propulsive efficiency [37]. With the target weight of the upcoming iteration computed, the value was checked against the operating empty weight. If the value happened to be lower than this, the analysis was considered completed, the returned weight was set to the operating empty weight, and the altitude of the current iteration was returned as the succeeding iteration was an invalid point.

As a final step before the numerical integration procedure proceeded onto its next iteration, the time and travelled distance were incremented:

$$t = t + dt \quad (14)$$

$$S = S + (V - V_{\text{wind}})dt \quad (15)$$

where t is the time required for the segment, which started counting from 0, S is the distance travelled during the segment in m , also counting from 0, V is the true airspeed, and V_{wind} is the windspeed [37].

Once the numerical iteration loop was completed the consumed fuel weight was calculated by subtracting the final aircraft weight from the initial value:

$$W_{\text{fuel}} = W_{\text{init}} - W_{\text{final}} \quad (16)$$

2.3.2 Descent-phase analysis

The descent analysis was similar in implementation to the climb segment calculation, but utilised a prescribed descent rate and was run with reverse time stepping. With this, the function was called with a known final weight (usually maximum landing weight), and it would compute the initial weight, time and distance for a target initial altitude.

As with the climb analysis, the algorithm begins at the specified initial condition and computes the instantaneous quantities. This differs slightly from the climb analysis and was carried out with the following steps:

1. Set the descent rate to the target value.
2. Convert the calibrated airspeed from the speed schedule into true airspeed.
3. Find the maximum continuous effective thrust and power from the thrust model.
4. Calculate the lift coefficient.
5. Request the corresponding drag coefficient from the aerodynamic model.
6. Compute the drag force.
7. Compute the required thrust for the target descent rate.
 - a. If the thrust required exceeds the thrust available, update the instantaneous descent rate based on the available thrust.
 - b. If the thrust required is less than 0, set the thrust required to 0.

The mathematical steps required to carry out steps 2–6 were explained in the climb-phase analysis. Regarding the computation of required thrust force, this was done with the following equation. It can be seen that the equation was similar to setting the thrust equal to drag (as would be done in a cruise segment), but the amount required is reduced because of the descent [37].

$$T_{\text{req}} = D - \frac{(\text{ROD}) \cdot W}{V} \quad (17)$$

where T_{req} is the required thrust in N, D is the drag force in N, ROD is the rate of descent in m/s, W is the aircraft weight in N and V is the true airspeed in m/s.

Furthermore, for the cases where the required thrust exceeded that which was available, the achievable rate of descent was computed (and used to override the target value for that iteration) as follows:

$$\text{ROD} = - \frac{(T_{\text{avail}} - D)V}{W} \quad (18)$$

where T_{avail} is the available thrust, equal to the combined maximum continuous thrust of the engines, in N [36].

With the instantaneous quantities computed, the values for the successive iteration were computed. Temporally, this referred to a ‘previous’ step (as the analysis was conducted from the final state to calculate the initial state), but algorithmically was the ‘next’ step. First, the altitude of this next step was computed with:

$$h_{i+1} = h_i - \text{ROD} \cdot dt \quad (19)$$

where h_{i+1} is the altitude of the next step, h_i is the altitude of the current step and dt is the timestep, equal in this case to -1 seconds. Note that the minus sign on the second term merely resulted from convention and resulted from the rate of descent quantity having the opposite sign of the rate of climb.

The weight of the next iteration was also computed, where the weight was increased by the amount of fuel that had been burned with one step of the descent:

$$W_{i+1} = W_i - \frac{P_{\text{req}}}{\eta_p} \text{SFC} \cdot dt \quad (20)$$

where W_{i+1} is the weight of the next step, W_i is the weight of the current step, SFC is the specific fuel consumption of the engine, η_p is the propulsive efficiency of the engines, and P_{req} is the required effective power from the propeller in W [35]. The required power was calculated with the following relationship:

$$P_{req} = T_{req} V \quad (21)$$

The weight value was then checked against the maximum takeoff weight of the aircraft, and if it exceeded this value then the weight was set to MTOW, and the current iteration's values were returned.

As a final step for each iteration, as with the climb analysis, the time and travelled distance were incremented. Once the numerical iteration was completed, the spent fuel value was also computed by taking the difference between the initial and final aircraft weights.

2.3.3 Cruise-phase analysis

The cruise segment analysis is ultimately similar to the climb segment analysis, involving similar numerical integration and forward time-stepping, but employed a different method to determine when the segment had been completed. Unlike the climb and descent segments, where a final altitude is the obvious desired data point, the cruise segment was developed to have three modes of terminating: a weight target, a time target or a distance target. With this, the cruise analysis continued to integrate (as long the weight didn't drop below OWE or the required thrust exceeded that available) until a specified weight was reached, or a time/distance value was exceeded.

As with the other numerical analysis schemes employed in this paper, the cruise-phase algorithm began each iteration by calculating the instantaneous quantities. This was carried out in the following order:

1. Convert the calibrated airspeed from the speed schedule into true airspeed.
2. Request the maximum continuous effective thrust from the thrust model.
3. Calculate the lift coefficient.
4. Request the corresponding drag coefficient from the aerodynamic model.
5. Compute the drag force.

The implementation of these five steps was described in the climb-phase analysis.

With both the drag force and available thrust known, the magnitude of the drag force was checked to ensure that it was below the available thrust threshold. If the drag force exceeded this value, then the analysis was completed, and the current iteration's values were returned.

Passing the drag force check, the weight for the succeeding iteration (one timestep ahead) was computed. This was done with the following relation:

$$W_{i+1} = W_i - \frac{P_{req}}{\eta_p} \text{SFC} \cdot dt \quad (22)$$

The required power was calculated as follows:

$$P_{req} = DV \quad (23)$$

where D is the drag force in N [37].

As with the climb analysis, the weight predicted by this forward stepping was compared against the operating empty weight of the aircraft. If the value was less than OWE, then the weight was set to equal OWE and the analysis was exited as the data point for the next point was invalid.

The remaining steps in the analysis aligned with the climb and descent analyses. For each iteration, the time and distance were incremented before the algorithm moved onto the next iteration. Once the exiting threshold was reached, be it the weight, time or distance mode, the consumed fuel was calculated from

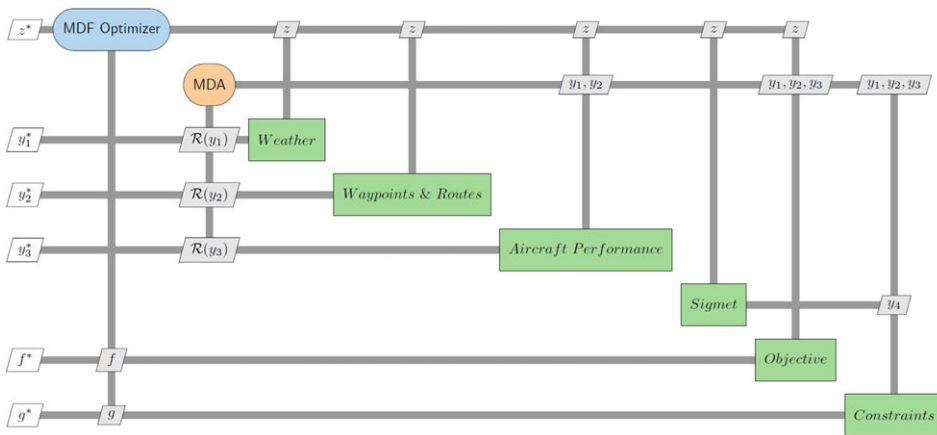


Figure 1. The XDSM [38] block diagram of the MDO process to optimise the flight trajectory.

the difference between initial and final weights. After this, the cruise analysis was considered completed and the function was exited.

3.0 MDO framework

In this paper, the MDF framework with a GA optimisation was implemented. This framework was developed using MATLAB and was utilised to find the optimum flight path for the aircraft. The algorithm was constructed by coupling the GA-based optimisation module with MAPLA’s performance module, weather information, SIGMET and pre-existing flight routes to provide the most optimum trajectory according to the fuel consumption and/or flight time. The GA MATLAB toolbox requires the following inputs: number of variables, lower and upper variable bounds, constraint functions, initial population matrix, population size and the objective function. The population size of the GA used in this study was set to 100 and the average relative change in the best fitness function value over maximum stall generations was equal to 1e-6.

With respect to the four different disciplines considered in this study including the weather model, SIGMET, ATC Waypoints and Routes, and the aircraft performance, the flowchart in Fig. 1 was suggested for the multi-disciplinary flight trajectory optimisation of the proposed aircraft. Accordingly, in order to run the system level optimiser, each level was analysed in sequence, with the outputs of each being used by the remaining disciplines. Finally, the flight trajectory was optimised based on the most optimum scenario to lower fuel consumption and/or flight time.

The method was outlined as follows and the corresponding XDSM block diagram [38] is shown in Fig. 1:

1. Model the weather information.
 - (I) Temperature model in the 4D space of longitude, latitude and altitude directions and time.
 - (II) Wind speed model in the 4D space.
 - (III) Wind direction model in the 4D space.
2. Get the SIGMET information and specify hazardous locations.
3. Model the ATC waypoints and routes.
4. Calculate the corresponding aircraft performance characteristics for different flight conditions and environments.

Table 1. The list of constraints considered for the proposed aircraft

Constraint	Description	Limits
W_{TO}	Aircraft max take-off weight, lb	5, 500lb
CG	Centre of gravity, %	$17 < CG < 30 \%$
$\delta_{r_{max}}$	Rudder deflection, deg	$0 \leq \delta_r \leq 30 \text{ deg}$
δ_e	Elevator deflection, deg	$-15 \leq \delta_e \leq 30 \text{ deg}$
δ_{flap}	Flap deflection, deg	$0 \leq \delta_{flap} \leq 30 \text{ deg}$
V	Aircraft speed, m/s	$V < 190 \text{ kt}$
h	Flight altitude, ft	$3,000 < h < 15,000 \text{ ft}$

5. Run the MDF-based optimisation.
6. Check for convergence with current goal.

3.1 Variables

In this study, the main concern was to find the most cost-efficient flight path for the proposed light aircraft and the corresponding variables were defined according to the requirements of each discipline. For the weather and SIGMET, the core variable was time. For ATC waypoints and routes, the corresponding variable was the pre-existing routes defined by different alternatives. The aircraft performance characteristics were found in accordance with the other three disciplines. Accordingly, having the information from the weather, SIGMET and the ATC waypoints and routes, the required performance data was generated.

3.2. Objective functions

As the main objective of this study was to find the most optimum scenario according to the fuel consumption and/or flight time, the objective functions were also defined such that minimum values were reported by the end. Hence, the minimum flight time and fuel consumption were defined by the following functions.

$$J_1(h, t, R) = \min(\text{Fuel}_{\text{climb}} + \text{Fuel}_{\text{cruise}} + \text{Fuel}_{\text{descend}} + \text{Fuel}_{\text{loiter}}) \quad (24)$$

$$J_2(h, t, R) = \min(\text{Time}_{\text{climb}} + \text{Time}_{\text{cruise}} + \text{Time}_{\text{descend}}) \quad (25)$$

where J_1 and J_2 are the cost objectives as a function of the flight altitude h , time t and the predefined route R , for fuel and time optimisations, respectively.

Aircraft characteristics were defined based on the constraints of the actual aircraft for weight, speed, centre of gravity location, control surfaces deflections and engine specifications. Table 1 presents the corresponding constraints.

In addition, the constraints associated with geographical location and altitude, as well as the pre-existing routes, are defined in Tables 2 and 3. The departure location for this demonstration was Thunder Bay, Canada while the destination was selected to be Sioux Lookout, Canada.

Finally, the corresponding data for temperature, wind speed and wind direction in the four-dimensional space is presented in Fig. 2(a) and (b) for two different altitudes of 10,000 and 18,000ft, respectively. The entire weather data for the altitudes from 3,000 to 18,000ft were gathered for the 24-hour time according to the geographical location in three different sets of 6:00 am to 17:00 pm, 17:00 pm to 21:00 pm and 21:00 pm to 6:00 am [24]. Accordingly, quadrilinear interpolation was implemented to find the weather information for each latitude, longitude and altitude direction at the specific time.

Table 2. The departure and destination specs

Constraint	Description	Departure (Thunder Bay, Canada)	Destination (Sioux Lookout, Canada)
Alt	Field elevation, ft	653ft	1,257ft
Lat	Latitude direction, deg	48.3609 deg	50.0978 deg
Lon	Longitude direction, deg	-89.2477 deg	-91.9220 deg

Table 3. The list of routes and corresponding characteristics of each one

Constraint	Description	Route 1	Route 2
Lat _A	Latitude direction leg A, deg	48.050 deg	48.5669 deg
Lon _A	Longitude direction leg A, deg	-89.5579 deg	-89.5296 deg
Magn _A	Magnetic course leg A, deg	232 deg	150 deg
Dist _A	Distance leg A, nm	33 nm	41 nm
Magn _B	Magnetic course leg B, deg	332 deg	133 deg
Dist _B	Distance leg B, nm	149 nm	106 nm

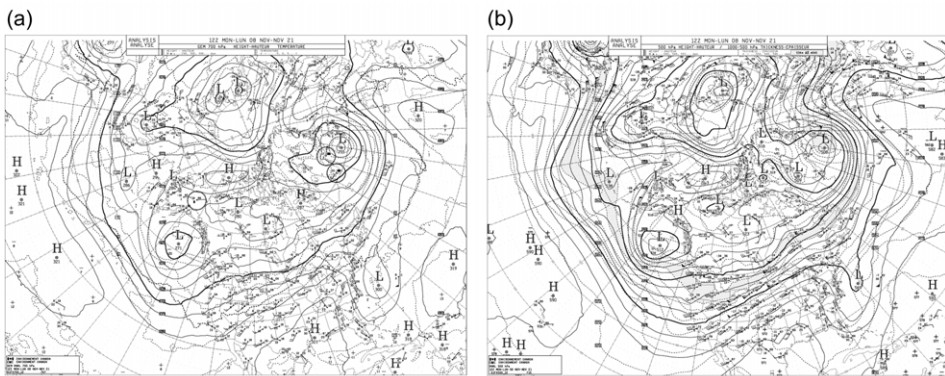


Figure 2. Weather data used for the flight from Thunder Bay, Canada to Sioux Lookout, Canada on 8 November 2021 for altitudes for (a) 10,000ft; (b) 18,000ft [25].

4.0 Results and discussion

In this section, the geometry of the proposed aircraft configuration modelled in MAPLA along with the performance characteristics and flight trajectory optimisation results are presented and compared with the known aircraft specifications taken from the flight manual of the Beechcraft G58 Baron.

4.1 Aircraft geometry

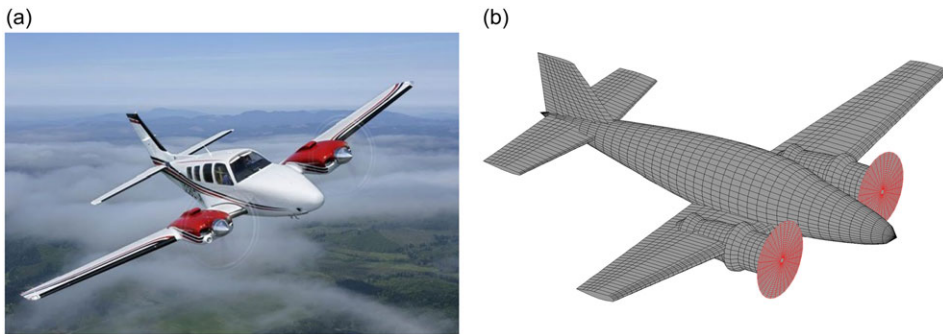
The geometry of the twin-engine Beechcraft G58 Baron aircraft configuration [39] and the one modelled in and simulated by MAPLA is presented in Fig. 3(a) and (b), respectively. The corresponding geometry values are also presented and described in Table 4.

4.2 Performance characteristics

This section documents the performance characteristics of the aforementioned twin-engine aircraft, presented for different flight conditions using the performance module of MAPLA. This information is presented as a time, fuel and distance associated with different flight conditions of climb, cruise and

Table 4. The Beechcraft G-58 Baron aircraft specs used to model the proposed aircraft in MAPLA [39]

Aircraft specs	Description	Value
l_w	Overall length, ft	29 ft 10 in
h_{aircraft}	Overall height, ft	9 ft 9 in
b_w	Wing span, ft	37 ft 10 in
i_w	Wing incidence at root, deg	4 deg
θ_w	Wing Twist, deg	-4 deg
Γ_w	Wing dihedral, deg	6 deg
c_w	Wing chord at root, ft	7 ft
c_{tw}	Wing chord at tip, ft	2 ft 11.5 in
AR_w	Wing Aspect Ratio	12.18
S_w	Wing area, sq ft	199.2 sq ft
b_h	Horizontal tail span, ft	15 ft 11 in
S_h	Horizontal tail area, sq ft	53.3 sq ft
S_v	Vertical tail area, sq ft	15.67 sq ft
P	Engine power, hp	300 hp
d_p	Propeller diameter, ft	6 ft 5 in
Y_p	Engine location in Y axis, ft	5 ft 10 in

**Figure 3.** (a) The Beechcraft G-58 Baron aircraft (Courtesy of Beechcraft) [40]. (b) The modelled aircraft using MAPLA.

descend for a typical flight from Thunder Bay, Ontario, Canada to Sioux Lookout, Ontario, Canada. In this section, the corresponding data for Route 1 and Route 2 shown in Fig. 4, taken from SkyVector [26] and using the weather information from NAVCanada [27], is presented and discussed in detail. For validation, the actual data according to the pilot flight manual of the Beechcraft G-58 Baron airplane was also presented and compared with the estimations from MAPLA.

Figure 5(a) through (c) show the estimated and actual climb flight characteristics of the proposed aircraft using MAPLA compared to the flight manual of the Beechcraft G58 Baron. Figure 5(a) presents the required time in minutes to reach the desired altitude in climb flight using Route 1 and Route 2. As can be seen, the data shown here are limited to 11,000 and 12,000ft for Route 1 and Route 2, respectively. This was done due to the limitations in the first-left distance, imposed by SkyVector [26]. As specified in Table 4, these were equal to 33 and 41nm, respectively. Following, Fig. 5(b) shows the required fuel in US gallons to reach the desired altitude in climb flight for the two routes. Finally, Fig. 5(c) shows the distance flown in nm to reach the desired altitude in climb flight.

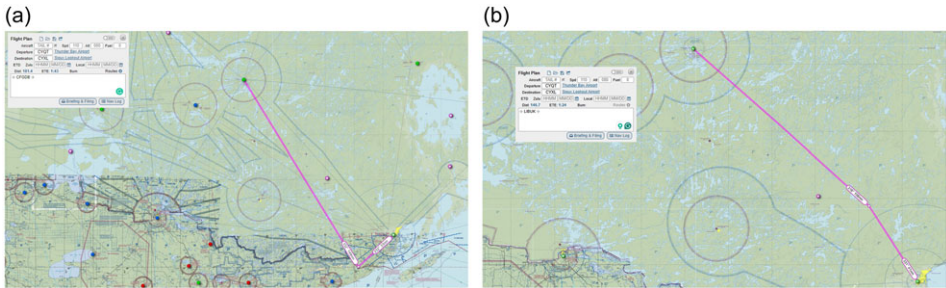


Figure 4. Pre-existing waypoints information for a flight from Thunder Bay, Canada to Sioux Lookout, Canada using (a) Route 1; (b) Route 2 [26].

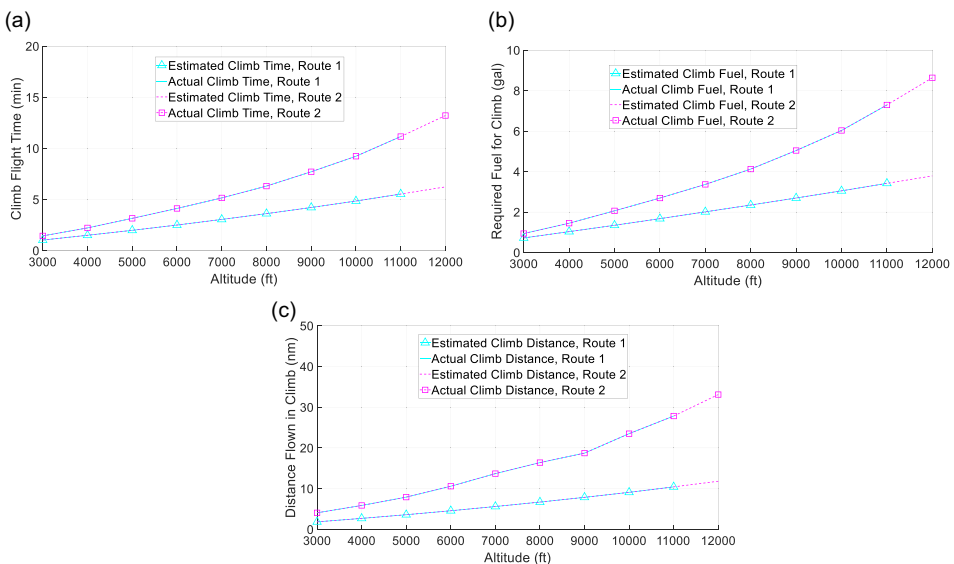


Figure 5. (a) The required time to reach the desired altitude in climb flight using Route 1 and Route 2; (b) the required fuel to reach the desired altitude in climb flight using Route 1 and Route 2; (c) the distance flown to reach the desired altitude in climb flight using Route 1 and Route 2, for a typical flight from Thunder Bay, Ontario, Canada to Sioux Lookout, Ontario, Canada using a Beechcraft G58 Baron aircraft modelled in MAPLA and compared with the flight manual data.

Figure 6(a) through Fig. 6(c) show the estimated and actual cruise flight characteristics of the proposed aircraft using MAPLA and flight manual of Beechcraft G-58 Baron. Similar to the climb plots, Fig. 6(a) presents the required cruise time in minutes for the for the two routes, Fig. 6(b) shows the required fuel for both, and finally, Fig. 6(c) plotted the distance flown in nm for the scenarios.

Figure 7(a) through Fig. 7(c) show the estimated and actual descend flight characteristics of the proposed aircraft using MAPLA and the flight manual of Beechcraft G-58 Baron. Figure 7(a) presents the required descent time in min, Fig. 7(b) shows the required fuel in U.S. gallons from each desired altitude, and lastly, Fig. 7(c) shows the distance flown in nm from each desired altitude in descend flight using Route 1 and Route 2.

Figures 8 and 9 show the estimated and actual total flight characteristics of the proposed aircraft in a typical flight from Thunder Bay, Ontario, Canada to Sioux Lookout, Ontario, Canada. Figure 8(a) represents the total required time in min considering each altitude using Route 1 and Route 2. Similarly,

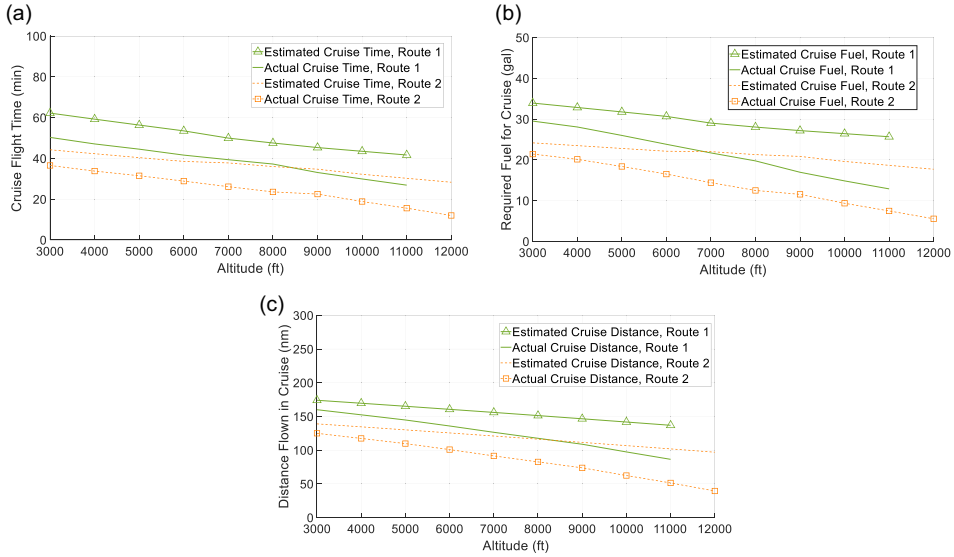


Figure 6. (a) The required cruise time at each desired altitude using Route 1 and Route 2; (b) the required fuel at each desired altitude using Route 1 and Route 2; (c) the distance flown at each desired altitude in cruise flight using Route 1 and Route 2, for a typical flight from Thunder Bay, Ontario, Canada to Sioux Lookout, Ontario, Canada using a Beechcraft G58 Baron aircraft modelled in MAPLA and compared with the flight manual data.

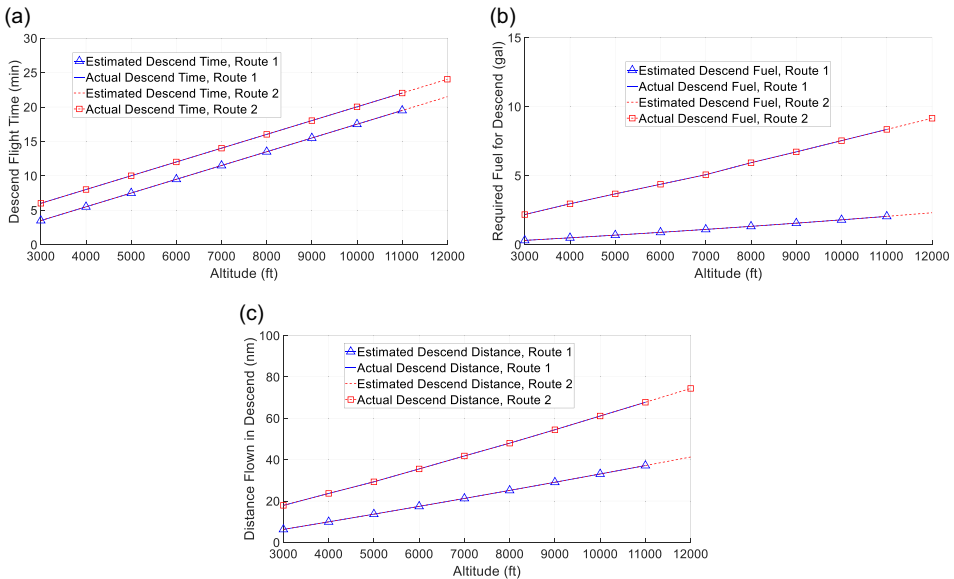


Figure 7. (a) The required descend time from each desired altitude using Route 1 and Route 2; (b) the required fuel from each desired altitude using Route 1 and Route 2; (c) the distance flown from each desired altitude in descend flight using Route 1 and Route 2, for a typical flight from Thunder Bay, Ontario, Canada to Sioux Lookout, Ontario, Canada using a Beechcraft G58 Baron aircraft modelled in MAPLA and compared with the flight manual data.

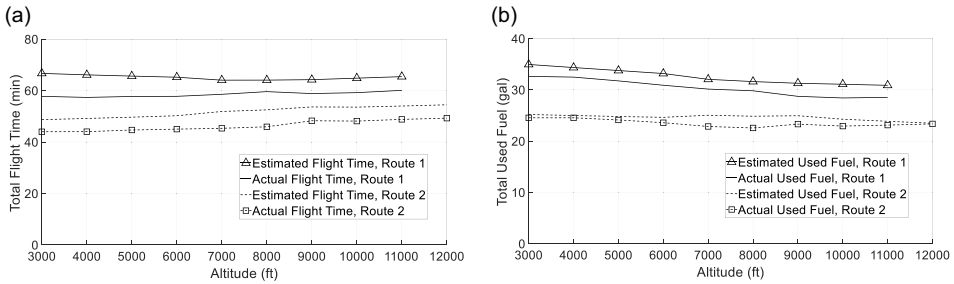


Figure 8. (a) The total required time considering each altitude using Route 1 and Route 2; (b) the total used fuel using each desired altitude for Route 1 and Route 2, for a typical flight from Thunder Bay, Ontario, Canada to Sioux Lookout, Ontario, Canada using a Beechcraft G58 Baron aircraft modelled in MAPLA and compared with the flight manual data.

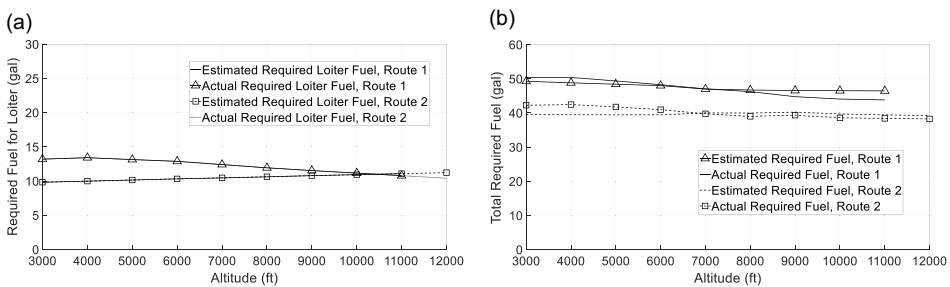


Figure 9. (a) The required fuel for loiter at each desired altitude using Route 1 and Route 2 considering 45 minutes loiter; (b) the total required fuel for each desired altitude using Route 1 and Route 2 considering 45 minutes for loiter and 4.5 US gallons fuel for the warm up and taxi on the ground for a typical flight from Thunder Bay, Ontario, Canada to Sioux Lookout, Ontario, Canada using a Beechcraft G58 Baron aircraft modelled in MAPLA and compared with the flight manual data.

Fig. 8(b) shows the total spent fuel in US gallons using each desired altitude. Figure 9(a) shows the required fuel in US gallons for loiter at each desired altitude using Route 1 and Route 2 considering 45 minutes for loiter. Figure 9(b) shows the total required fuel in US gallons for each desired altitude using Route 1 and Route 2 considering 45 minutes for loiter and 4.5 US gallons fuel for the warmup and taxi on the ground suggested by the aircraft manual for this aircraft type.

4.3 Flight trajectory optimisation

In this section, with respect to the MDO framework discussed in Fig. 1 and using the aforementioned disciplines the optimised altitude for each route was suggested for the Beechcraft G-58 Baron aircraft. Considering the results achieved for both routes, the better of the two was suggested for the flight from Thunder Bay, Ontario, Canada to Sioux Lookout, Ontario, Canada at a specific day and time. It should be noted that the optimisation process was completed for the day of 8 November 2021, and is shown here for the departure time of 10:00 am.

Figures 10 shows the optimised flight altitude against the distance travelled at each flight phase of climb, cruise and descend using estimated and actual data for Route 1 and Route 2. For Route 1, the optimised flight altitude using the estimated performance calculations from MAPLA was to 9,500ft, while using the actual performance data from the flight manual of the Beechcraft G-58 Baron aircraft

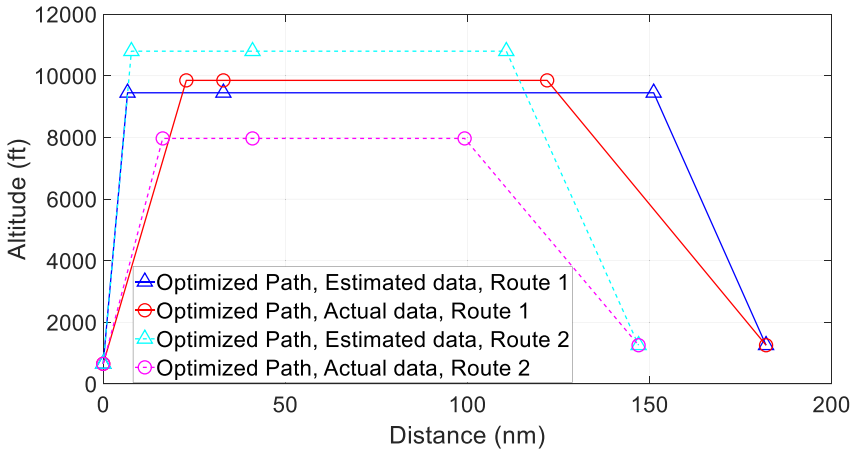


Figure 10. The optimised flight altitude against the distance travelled at each flight phase of climb, cruise and descend using estimated and actual data for Route 1 and Route 2.

suggested 9,800ft. For Route 2, the optimised flight altitude using the estimated performance calculations from MAPLA is equal to 10,800ft, while using the actual performance data from the flight manual of the Beechcraft G-58 Baron aircraft suggested 8,000ft.

In investigating the Route 2 discrepancy, with respect to Figs 8 and 9, it was found that the required fuel and total flight time varied very little above 8,000ft for both estimated and actual results. This minimal variation caused the optimiser to select different optimised altitudes, resulting in discrepancies between the MAPLA results and those provided by the flight manual.

4.4 Future works and improvements

Two main improvements were outlined to greatly enhance the predictive accuracy of the included modules: non-constant propulsive efficiency and accounting for change in the centre of gravity [34, 38].

Starting with the propulsive efficiency, the current implementation employs an assumption where propulsive efficiency remains unchanged across all slight segments and speeds. This was the traditional modelling approach, and as such, was replicated for this algorithm. In actuality, however, the efficiency is a function of true airspeed, and this assumption results the prediction of optimal flight speeds lower than would be observed during actual flight [34]. In a future version of this analysis, the constant propulsive efficiency will be preplaced by an efficiency vs. true airspeed curve, which will be accessed during each step of the numerical integration schemes employed by the segment calculators. Producing such a curve manually is expected to be prohibitively time-consuming, and as such this will involve the digitising of empirical propeller curves for static and inflight thrust to automate this calculation, with the user instead being required to supply the propellers characteristics [38].

The second major improvement to be pursued will be accounting for the change in CG position over the course of a segment. In the current implementation, the longitudinal position of the centre of gravity is assumed to be constant over an entire segment. Reality generally disagrees with this, however, as burning fuel will remove mass from the aircraft and cause the CG to shift. Accounting for this change will allow the analysis to take advantage of the aerodynamic model's drag offset capability and develop a more accurate prediction of the drag force at each given moment of the flight [34].

Figure 11 shows the 3-dimensional representation of the optimized flight altitude against the longitude and latitude directions at each flight phase of climb, cruise and descend using estimated and actual data for Route 1 and Route 2.

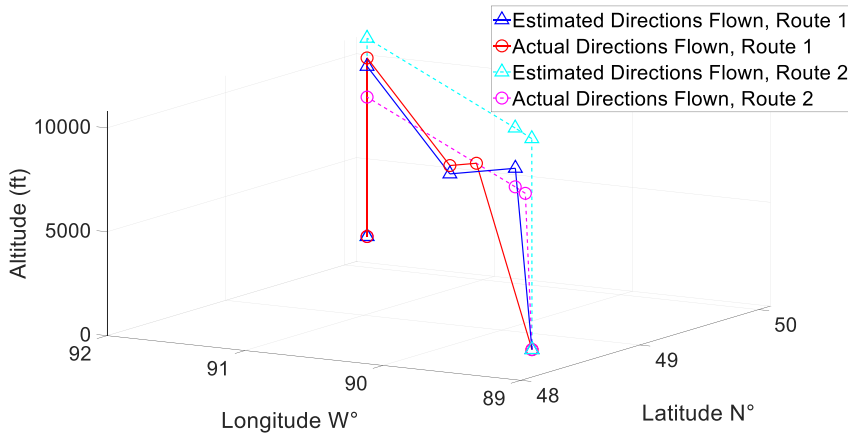


Figure 11. The 3D representation of the optimised flight altitude against the longitude and latitude directions at each flight phase of climb, cruise and descend using estimated and actual data for Route 1 and Route 2.

5.0 Conclusion

In conclusion, the proposed multidisciplinary approach provided a standalone flight path optimisation tool to choose the scenario that best accomplishes the cost objectives of an airline (e.g., fuel, time etc.). In this work, three disciplines were considered including the weather model and SIGMET, ATC waypoints and routes, as well as the aircraft performance using SAFPO's own performance calculator. The aerodynamic characteristics of the aircraft were determined using a validated semi-empirical programme called MAPLA developed for light aircraft analysis. With respect to the results compared with an actual Beechcraft Baron G58 flight manual information, the proposed approach may improve the flight path optimisation of light aircraft to reduce the operational costs of small and local airlines.

Author contributions. Conceptualisation, M.R. and J.C.; Methodology, M.R., J.B., D.N. and J.C.; Software, M.R. and J.K.; Formal analysis, M.R. and D.N.; Writing – original draft, M.R, J.B.; Preparation, M.R, J.B.; Data curation, M.R, J.B.; Writing – review and editing, J.B., D.N. and J.C. All authors have read and agreed to the published version of the manuscript.

Funding. This work was supported by Mitacs through the Mitacs Accelerate Program (reference number: IT16648) and Columbiad Launch Services Inc.

Competing interests. The authors declare none.

References

- [1] Dharmaseelan, A. and Adistambha, K.D. Flight plan optimization, *Multisensor, Multisource Information Fusion: Architectures, Algorithms, and Applications 2015*, Vol. 949807, 2015. <https://doi.org/10.1117/12.2178144>
- [2] Tian, Y., He, X., Xu, Y., Wan, L. and Ye, B. 4D trajectory optimization of commercial flight for green civil aviation, *IEEE Access*, 2020, **8**, pp 62815–62829. <https://doi.org/10.1109/ACCESS.2020.2984488>
- [3] Altus, S. Effective Flight Plans Can Help Airlines Economize. *Aero Q.* – Boeing, 27–30, 2009. Retrieved from http://www.boeing.com/commercial/aeromagazine/articles/qtr_03_09/pdfs/AERO_Q309_article08.pdf
- [4] Uçan, F. and Altılar, D.T. Using genetic algorithms for navigation planning in dynamic environments, *Appl. Comput. Intell. Soft Comput.*, 2012, pp 1–16. <https://doi.org/10.1155/2012/560184>
- [5] Al-Jarrah, M.A. and Hasan, M.M. HILS setup of dynamic flight path planning in 3D environment with flexible mission planning using Ground Station, *J. Franklin Inst.*, 2011, **348**, pp 45–65. <https://doi.org/10.1016/j.jfranklin.2009.02.012>
- [6] Ramée, C., Kim, J., Deguignet, M., Justin, C., Briceno, S. and Mavris, D. Aircraft flight plan optimization with dynamic weather and airspace constraints, *Int. Conf. Res. Air Transp.*, 2020, pp 1–8.
- [7] Ghazi, G., Botez, R.M., Bourrelly, C. and Turculet, A.-A. Method for calculating aircraft flight trajectories in presence of winds, *J. Aerosp. Inf. Syst.*, 2021, **18**, pp 442–463. <https://doi.org/10.2514/1.i010879>

- [8] Li, C. and Hansman, R.J. Preliminary development of a cruise altitude and speed optimization decision support tool, *2018 Aviation Technology, Integration, and Operations Conference*, 2018, pp 1–13. <https://doi.org/10.2514/6.2018-3513>.
- [9] Rosenow, J., Strunck, D. and Fricke, H. Trajectory optimization in daily operations, *CEAS Aeronaut. J.*, 2018, **11**, pp 333–343.
- [10] Wang, Y., Sun, H., Zhu, J. and Zhu, B. Optimization model and algorithm design for airline fleet planning in a multi-airline competitive environment, *Math. Probl. Eng.*, 2015. <https://doi.org/10.1155/2015/783917>
- [11] Dancila, B.D., Beulze, B. and Botez, R.M. Flight phase and altitude-dependent geometrical vertical flight plan optimization minimizing the total number of vertical plan segments, *Proc. Inst. Mech. Eng. Part G J. Aerosp. Eng.*, 2019, **233**, pp 4825–4838. <https://doi.org/10.1177/0954410019832127>
- [12] Thayer, R.H. and Bjorke, P. Concept of operations for the next generation air transportation system, *Encycl. Softw. Eng.*, 2011. <https://doi.org/10.1002/0471028959.sof055>
- [13] Degarmo, M.T. (2004). Issues Concerning Integration of Unmanned Aerial Vehicles in Civil Airspace.
- [14] Weibel, R.E. and Hansman, R.J. Safety considerations for operation of unmanned aerial vehicles in the national airspace system, *Transportation (Amst)*, 2005, **37**, pp 26–30.
- [15] Woods, S.E., Vivona, R.A., Henderson, J., Wing, D.J. and Burke, K.A Traffic aware planner for cockpit-based trajectory optimization, *16th AIAA Aviation Technology, Integration, and Operations Conference*, 2016, pp 1–13. <https://doi.org/10.2514/6.2016-4067>
- [16] Lewis, T.A., Burke, K.A., Underwood, M.C. and Wing, D.J. Weather design considerations for the tasar traffic aware planner, *AIAA Aviation 2019 Forum*, 2019, pp 1–16. <https://doi.org/10.2514/6.2019-3616>
- [17] Underwood, M.C., Lewis, T.A. and Barney, T.L. In-flight evaluation of the traffic aware planner on the NASA hu-25a guardian aircraft, *AIAA Aviation 2019 Forum*, 2019, pp 1–13. <https://doi.org/10.2514/6.2019-3615>
- [18] Barney, T.L., Underwood, M.C. and Buck, B.K. Simulation and flight test environments for the tasar traffic aware planner, *AIAA Aviation 2019 Forum*, 2019, pp 1–10. <https://doi.org/10.2514/6.2019-3614>
- [19] Woods, S.E., Vivona, R.A., Roscoe, D.A., LeFebvre, B.C., Wing, D.J. and Ballin, M.G. A cockpit-based application for traffic aware trajectory optimization, *AIAA Guidance, Navigation, and Control Conference*, 2013, pp 1–14. <https://doi.org/10.2514/6.2013-4967>
- [20] NASA's Technology Transfer Program. Flight Optimization System (FLOPS) Software, LAR-18934-1, 2021. <https://software.nasa.gov/software/LAR-18934-1>
- [21] Wells, D.P., Horvath, B.L. and McCullers, L.A. The Flight Optimization System Weight Estimation Method. NASA Tech. Memo. 219627. TM-2017-21, 2017.
- [22] Martins, J.R.R.A. and Lambe, A.B. Multidisciplinary design optimization: A survey of architectures, *AIAA J.*, **51**, (9), 2013, pp 2049–2075. <https://doi:10.2514/1.J051895>
- [23] Simpson, T.W., Mauery, T.M., Korte, J.J. and Mistree, F. Comparison of response surface and kriging models for multidisciplinary design optimization, *7th AIAA/USAF/NASA/ISSMO Symposium on Multidisciplinary Analysis and Optimization*, 1998, pp 381–391. <https://doi:10.2514/6.1998-4755>
- [24] Yi, S.I., Shin, J.K. and Park, G.J. Comparison of MDO methods with mathematical examples, *Struct. Multidiscip. Optim.*, 2008, **35**, pp 391–402. <https://doi.org/10.1007/s00158-007-0150-2>
- [25] NavCanada. NavCanada website, n.d. Retrieved November, 2021, from https://flightplanning.navcanada.ca/cgi-bin/CreePage.pl?Langue=anglais&NoSession=NS_Inconnu&Page=forecast-observation&TypeDoc=html
- [26] SkyVector. SkyVector Aeronautical Charts, n.d. Retrieved November, 2021, from <https://skyvector.com/>
- [27] Rostami, M. and Bagherzadeh, S.A. Development and validation of an enhanced semi-empirical method for estimation of aerodynamic characteristics of light, propeller-driven airplanes, *Proc. Inst. Mech. Eng. Part G J. Aerosp. Eng.*, 2018, **232**, pp 638–648. <https://doi.org/10.1177/0954410016683415>
- [28] Rostami, M. and Chung, J. Multidisciplinary Analysis Program for Light Aircraft (MAPLA), *Proceedings of the Canadian Society for Mechanical Engineering International Congress*, Charlottetown, PE, Canada, 2021, pp 27–30. <https://doi.org/10.32393/csme.2021.92>
- [29] Rostami, M., Chung, J. and Neufeld, D. Vertical tail sizing of propeller-driven aircraft considering the asymmetric blade effect, *Proc. Inst. Mech. Eng. Part G J. Aerospace Eng.*, 2022, **236**, (6), pp 1184–1195. <https://doi.org/10.1177/09544100211029450>
- [30] Rostami, M., Chung, J. and Park, H.U. Design optimization of multi-objective proportional–integral–derivative controllers for enhanced handling quality of a twin-engine, propeller-driven airplane, *Advances in Mechanical Engineering*, 2020, **12**, (6). <https://doi.org/10.1177/1687814020923178>
- [31] Rostami, M., Bardin, J., Neufeld, D. and Chung, J. A multidisciplinary possibilistic approach to size the empennage of multi-engine propeller-driven light aircraft, *Aerospace*, 2022, **9**, (3), p 160. <https://doi.org/10.3390/aerospace9030160>
- [32] Rostami, M., Bardin, J., Neufeld, D. and Chung, J. EVTOL tilt-wing aircraft design under uncertainty using a multidisciplinary possibilistic approach, *Aerospace*, 2023, **10**, (8), p 718. <https://doi.org/10.3390/aerospace10080718>
- [33] Oyama, Y., Rostami, M. and Chung, J. Conceptual design and analysis of a box fan-in-split-wing tiltrotor EVTOL aircraft, *Aircraft Eng. Aerospace Technol.*, 2024. <https://doi.org/10.1108/AEAT-06-2023-0167>
- [34] Cavcar, A. Climb performance of piston-propeller airplane with cambered wing and variable propeller efficiency, *J. Aircraft*, 2011, **48**, (5), pp 1701–1707.
- [35] Cavcar, M. The International Standard Atmosphere, n.d. Retrieved from <http://fisicaatmo.at.fcen.uba.ar/practicas/ISAweb.pdf>
- [36] Massachusetts Institute of Technology. Aircraft Range: The Breguet Range Equation, n.d. Retrieved from <https://web.mit.edu/16.unified/www/FALL/thermodynamics/notes/node98.html>

- [37] Lan, C.-T.E. and Roskam, J. *Airplane Aerodynamic and Performance*, DARcorporation, 2011, Lawrence, Kansas.
- [38] Lambe, A.B. and Martins, J.R.R.A. Extensions to the design structure matrix for the description of multidisciplinary design, analysis, and optimization processes, *Struct. Multidiscip. Optim.*, 2012, **46**, (2), pp 273–284. <https://doi.org/10.1007/s00158-012-0763-y>.
- [39] Hawker Beechcraft Corporation. Model G58 Baron, Pilot's Operating Handbook and FAA Approved Airplane Flight Manual, P/N 58-590000-67, Original Issue - November, 2005.
- [40] Textron Aviation Inc. Model G58 Baron, n.d. Retrieved from <https://beechcraft.txtav.com/en/baron-g58>